



LETTER

New E' centers in neutron-irradiated α -quartz

To cite this article: R. I. Mashkovtsev and Y. Pan 2016 *EPL* **113** 64004

View the [article online](#) for updates and enhancements.

You may also like

- [Out-of-equilibrium fluctuations in stochastic long-range interacting systems](#)
Shamik Gupta, Thierry Dauxois and Stefano Ruffo
- [Generalized Rabi models: Diagonalization in the spin subspace and differential operators of Dunkl type](#)
Alexander Moroz
- [Internal one degree of freedom is sufficient to induce exact decoherence](#)
Eric A. Galapon

New E' centers in neutron-irradiated α -quartz

R. I. MASHKOVTSSEV^{1(a)} and Y. PAN^{2(b)}

¹ *V.S. Sobolev Institute of Geology and Mineralogy SB RAS - 630090 Novosibirsk, Russia*

² *Department of Geological Sciences, University of Saskatchewan - Saskatoon, Saskatchewan, S7N 5E2 Canada*

received 7 March 2016; accepted in final form 1 April 2016

published online 12 April 2016

PACS 42.70.Ce – Glasses, quartz

PACS 61.72.jd – Defects and impurities in crystals; microstructure Vacancies

PACS 61.72.J- – Points defects and defect clusters

Abstract – Several E' -type defects have been revealed in neutron-irradiated natural and synthetic α -quartz by using electron paramagnetic resonance (EPR) spectroscopy. For the known E'_2 center the primary spin Hamiltonian parameter matrices \mathbf{g} and $\mathbf{A}^{(29\text{Si})}$ (hyperfine interaction with ^{29}Si) have been refined and provide compelling evidence for spin trapping on the long-bond Si atom. The EPR spectra of the new E'_{11} center demonstrate that the super-hyperfine structure arises from the interaction with ^{27}Al , the first-ever example of Al-associated E' centers in crystalline quartz. The matrices \mathbf{g} and $\mathbf{A}^{(29\text{Si})}$ of E'_{11} and another new center (E'_{12}) support the forward-oriented configuration proposed for the E'_α center in amorphous silica.

Copyright © EPLA, 2016

Introduction. – Silica and α -quartz are important materials for traditional industries as well as high-tech electronic, optical and solar-energy applications. Many of these applications either require the materials to be resistant to the exposure of radiation or make direct use of specific radiation-induced point defects. The most common radiation point defects in crystalline quartz and amorphous silica are those associated with oxygen vacancies (so-called E' centers with electron spin $S = 1/2$ and E'' with $S = 1$; for recent reviews, see refs. [1,2]). The interaction of two neighboring E' centers results in the E'' centers and among these triplet centers the most salient feature is their stability at room temperature (RT) [3,4]. The E'' centers are characterized by hyperfine interactions (HFI) with two ^{29}Si nuclei and their HF values may be either about a half or a full integer of those for the E'_1 center depending on the exchange interaction between the two centers [4]. This fact is best demonstrated by the E''_9 center for which the most complete set of spin Hamiltonian parameters has been determined [5]. In crystalline quartz several E' centers are known: E'_1 [6], E'_2 (I, II) [7,8], E'_4 [9], $E'_{9,10}$ [1,10], and Ge E' [11,12]. Similarly, analogous defects including the E' -type centers with spin trapped on B, Al, P, Ge, and Sn have been observed in glasses [13]. One notable exception is the orthorhombic E'_α center in amorphous silica which is characterized by an anomalously

large isotropic ^{29}Si HFI (~ 49 mT) [14] and does not have any corresponding analog in crystalline quartz. From the very beginning the point defects in quartz samples were effectively produced with neutron fluxes [6,15]. Later it was shown that besides $E'_{1,2}$ centers, fast neutrons produced a number of other defects for which spin Hamiltonian parameters have not been determined [16,17]. In ancient flints and natural quartz grains additional E' -type EPR signals were observed at $g \approx 2$ but could not be identified with any reported E' centers [18,19]. Interestingly the E'_2 center featuring a long traverse relaxation time T_2 of $260 \mu\text{s}$ at 60 K and well-separated energy levels arising from the proton-coupled electron-nuclear structure has been proposed as a candidate for quantum memory in quantum computing [20]. Therefore, the investigations of the E' defects in quartz not only are still analytical challenges but also have high-tech applications. In this contribution we present a detailed EPR investigation on new E' centers in neutron-irradiated quartz.

Results and discussion. – For EPR investigations four samples with typical dimensions about $3 \times 5 \times 6 \text{ mm}^3$ in the X , Y , and Z directions, respectively, were cut from natural and synthetic crystals. Two samples (natural and synthetic) were irradiated with a fluence of $5 \times 10^{16} \text{ n/cm}^{-2}$ and two other samples with a fluence of $5 \times 10^{17} \text{ n/cm}^{-2}$ (neutron flux $> 1 \text{ MeV}$) in the Research Reactor Facility at Tomsk Polytechnic University. Transparent original crystals turned to smoke (natural sample)

^(a)E-mail: rim@igm.nsc.ru

^(b)E-mail: yuanming.pan@usask.ca

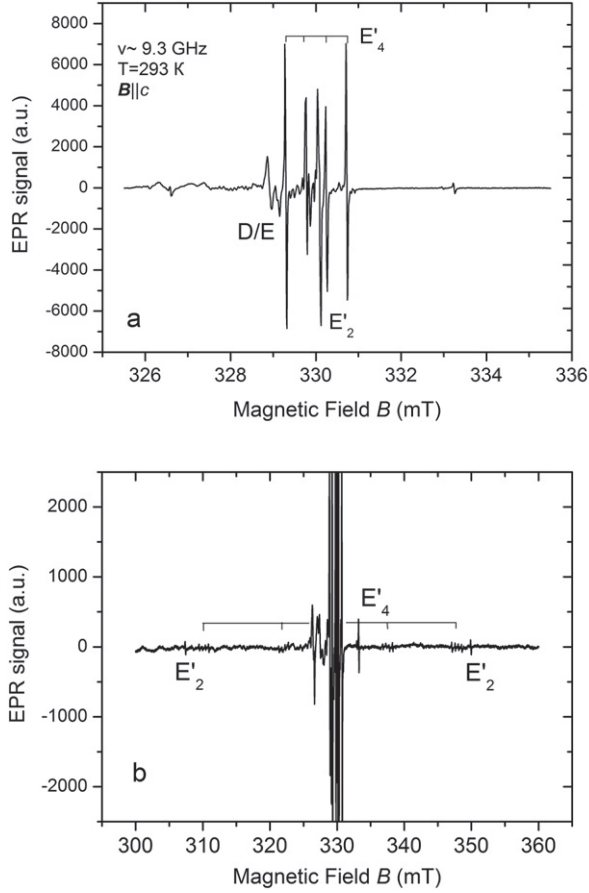


Fig. 1: EPR spectra taken with $\mathbf{B} \parallel c$ and at ~ 9.3 GHz for neutron-irradiated (fluence of 5×10^{16} n/cm $^{-2}$) synthetic α -quartz. (a) Central region of the spectrum showing the D/E hole centers and the main lines of centers E'_2 and E'_4 (b) Full spectrum with the ^{29}Si HF lines indicated for centers E'_2 and E'_4 .

and grey colour (synthetic sample) after irradiation. EPR spectra were measured at RT on a Radiopan SE/X 2543 spectrometer with a built-in NMR magnetometer. The sample was fastened on a home-built goniometer allowing two-axis rotation of the crystal in the cavity. The MgO:Cr or MgO:Mn reference materials were co-mounted with the sample and measured simultaneously to determine the microwave frequency that was slightly varied during the rotation of the crystal. Because of signal saturation the microwave power was reduced to 0.6 mW when the spectra of E' centers were collected. To investigate the thermal stability of defects the natural sample irradiated with a dose of 5×10^{17} n/cm $^{-2}$ was sequentially annealed at different temperatures for 15 min each in an oven.

Before irradiation no EPR signal was observable at RT. Figures 1 and 2 show that the EPR spectra at $\mathbf{B} \parallel c$ of the samples irradiated with the fluence of 5×10^{16} n/cm $^{-2}$ contain only known paramagnetic centers [1,2]. Two proton-associated oxygen deficient centers, E'_2 with ^{29}Si HF splitting of 42.5 mT and E'_4 with two pairs of quartets

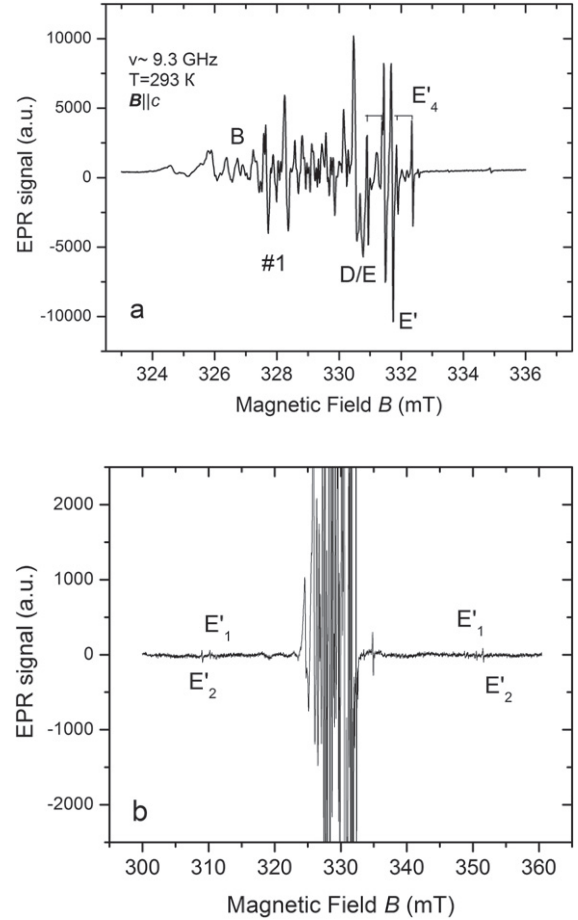


Fig. 2: EPR spectra taken with $\mathbf{B} \parallel c$ and at ~ 9.3 GHz for neutron-irradiated (fluence of 5×10^{16} n/cm $^{-2}$) natural α -quartz. (a) Central region of the spectrum showing the #1, #3, B and D/E hole centers and the main lines of centers E'_4 , and additional lines for other E' centers. (b) Full spectrum with the ^{29}Si HF lines indicated for centers E'_1 and E'_2 .

divided into two $^{29}\text{Si}_{1,2}$ splittings of 37.7 and 15.5 mT, dominate in the synthetic sample (fig. 1). In addition, the E'_1 center with ^{29}Si HF splitting of 40.35 mT is observed in the natural sample (fig. 2). The hole-like centers such as #1, #3, B and D/E [21,22] and other unreported centers are well observed in the natural sample (fig. 2(a)). In contrast only hole-like centers D/E [23] are clearly observed in the synthetic sample (fig. 1(a)).

Figures 3 and 4 show that the EPR spectra collected for the samples irradiated with the fluence of 5×10^{17} n/cm $^{-2}$ are different from those of their lower-fluence counterparts. The D/E defects are now dominant among the hole-like centers. Also the intensity of E' centers become much stronger. Moreover, the EPR spectra indicate that new paramagnetic defects are present in addition to the known hole-like and $E'_{1,2,4}$ centers. With the applied field $\mathbf{B} \parallel c$ the g -factors of the new E'_{11} and E'_{12} centers are both close to 2.001, so that the main lines of these centers are superimposed in the relevant B region (figs. 3(a) and 4(a)). But in the expanded range for $E'_{11,12}$ centers, the nar-

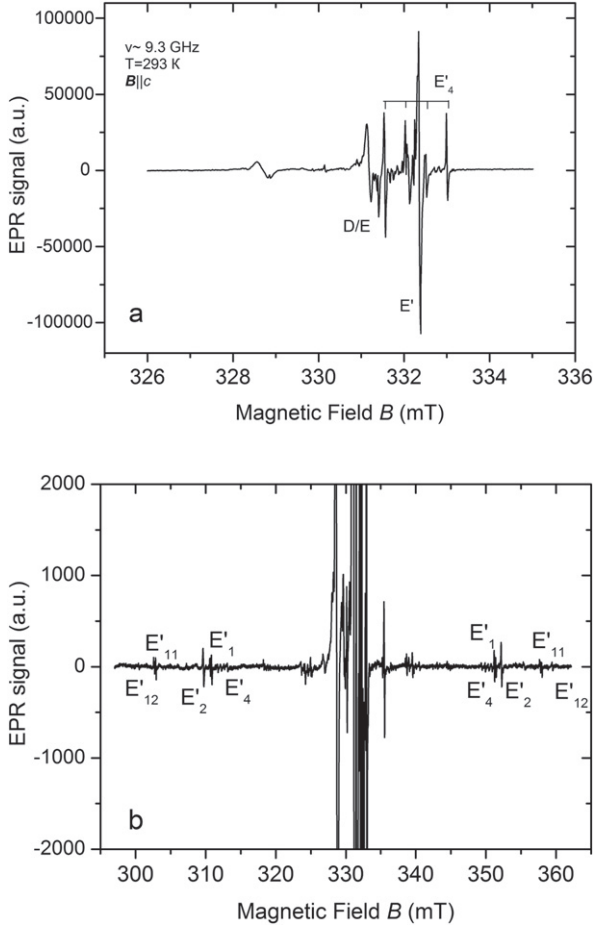


Fig. 3: EPR spectra taken with $\mathbf{B}\parallel c$ and at ~ 9.3 GHz for neutron-irradiated (fluence of 5×10^{17} n/cm $^{-2}$) synthetic α -quartz. (a) Central region of the spectrum showing the D/E hole centers and the main lines of centers E'_4 , and additional lines for other E' centers. (b) Full spectrum with the ^{29}Si HF lines indicated for centers $E'_{1,2,4}$ and $E'_{11,12}$.

row lines (measured width $\Delta B_{\text{pp}} \sim 0.03$ mT) of ^{29}Si HFS are well observed (see figs. 3(b) and 4(b)). HF splitting is 59.02 mT for the E'_{12} center and about 55.1 mT for the E'_{11} center. The set of E'_{11} lines (see insets in fig. 4(b)) is similar to the ^{27}Al super-hyperfine structure (SHFS) observed for the D/E centers in the skew orientations with a coupling value ~ 0.1 mT [23]. Also additional ^{29}Si HF lines that we did not investigated herein are observed (figs. 3(b) and 4(b)). For example, a pair of single lines with splitting of 40.78 mT at the outside of the $^{29}\text{Si}E'_1$ lines and another pair of weak lines with splitting of 48.18 mT indicate two unknown E' -type centers. Furthermore, two sets of lines with a distance of about 26.1 mT between them and probably associated with ^{27}Al SHFS are observed in the natural sample (fig. 4(b)). The inner $^{29}\text{Si}_2$ HF quartets of the E'_4 center are partially revealed by another set of lines with a distance of approximately 14.5 mT in both synthetic and natural samples (figs. 3(b), 4(b)).

The $E'_{2,4}$ and E'_{12} centers were bleached after heating at 150 $^\circ\text{C}$ and 200 $^\circ\text{C}$, respectively. The two sets of lines

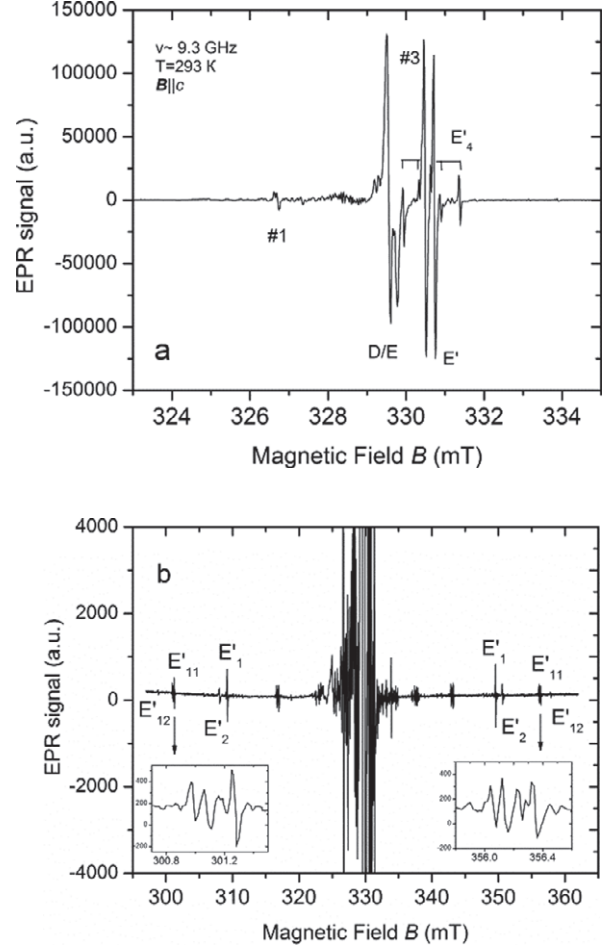


Fig. 4: EPR spectra taken with $\mathbf{B}\parallel c$ and at ~ 9.3 GHz for neutron-irradiated (fluence of 5×10^{17} n/cm $^{-2}$) natural α -quartz. (a) Central region of the spectrum showing the #1, #3, and D/E hole centers and the main lines of centers E'_4 , and additional lines for other E' centers. (b) Full spectrum with the ^{29}Si HF lines indicated for centers $E'_{1,2}$ and $E'_{11,12}$. In the insets the SHFS for the E'_{11} center is shown.

related to the ^{27}Al SHFS, including that of the E'_{11} center vanished after annealing at 275 $^\circ\text{C}$ when the E'_1 center was abruptly increased.

For the natural quartz irradiated with the fluence of 5×10^{17} n/cm $^{-2}$ the EPR spectra were recorded through 5° intervals when the crystal was rotated in the yz plane (*i.e.* around the a -axis). The right direction of rotation was controlled using the known angular variation of the ^{29}Si HF lines of the E'_1 center [1]. This result demonstrates that our quartz samples are right-handed crystals (see [2] on the handedness of quartz). The crystal-rotation line-position curves for the large ^{29}Si HFS are shown in fig. 5. The hyperfine structure of the E' centers can be described by spin Hamiltonian

$$H = \beta_e \mathbf{B}^T \cdot \mathbf{g} \cdot \mathbf{S} + \mathbf{S}^T \cdot \mathbf{A} \cdot \mathbf{I} - \beta_n \mathbf{B}^T \cdot \mathbf{g}_n \cdot \mathbf{I}, \quad (1)$$

with $S = 1/2$ and $I = 1/2$ for ^{29}Si nucleus. \mathbf{g} , \mathbf{A} , and \mathbf{g}_n are the electronic Zeeman splitting matrix, the HF

Table 1: Best-fit spin Hamiltonian matrices for the E' center in neutron-irradiated natural quartz at ca. 293 K and ~ 9.3 GHz. For E'_{11} matrices \mathbf{g} and $\mathbf{A}^{(29\text{Si})}$ were evaluated by line position difference minimization of 219 data points (73 for each of the 3 sites), sum of weighting factors = 193.3, and the root-mean square deviation (RMSD) of the final line position = 0.03 mT. For E'_{12} matrices \mathbf{g} and $\mathbf{A}^{(29\text{Si})}$ were evaluated by line-position difference minimization of 198 data points (66 for each of the 3 sites), sum of weighting factors = 197, and final line-position RMSD = 0.016 mT. For the E'_2 matrices \mathbf{g} and $\mathbf{A}^{(29\text{Si})}$ were evaluated by line-position difference minimization of 217 data points (72 for each of the 3 sites), sum of weighting factors = 211.6, and final line-position RMSD = 0.017 mT. For the E'_2 matrix $\mathbf{A}^{(1\text{H})}$ was evaluated by line-position difference minimization of 115 data points, sum of weighting factors = 73.9, and final line-position RMSD = 0.02 mT. θ is the polar angle from the c -axis; φ is the azimuthal angle relative to the a -axis. $(\theta_k^\circ, \varphi_k^\circ)$ is equivalent to $(180 - \theta_k^\circ, 180 + \varphi_k^\circ)$. The numbers within parentheses indicate the estimated uncertainties in the preceding numbers.

Center	Matrix \mathbf{Y}			k	Principal values Y_k	Principal directions		
						θ_k°	φ_k°	
E'_{11}	\mathbf{g}	2.00142(1)	0.00067(1)	-0.00058(1)	1	2.00184(1)	115.8(4)	11.5(3)
			1.99976(1)	0.00049(1)	2	2.00097(1)	35.5(4)	58.9(5)
				2.00087(1)	3	1.99925(1)	67.3(2)	293.1(2)
	$\mathbf{A}^{(29\text{Si})}$ (mT)	50.206(3)	0.405(3)	1.317(2)	1	55.375(2)	21.42(2)	45.16(6)
			50.264(3)	1.309(2)	2	49.921(3)	69.6(2)	244(2)
				54.646(2)	3	49.821(3)	96.3(5)	332(1)
E'_{12}	\mathbf{g}	2.00043(2)	0.00082(1)	-0.00035(2)	1	2.00171(2)	144.5(8)	256(1)
			2.00040(2)	0.00077(2)	2	2.00109(2)	64(1)	209.1(7)
				2.00124(1)	3	1.99927(2)	67.8(3)	311.1(5)
	$\mathbf{A}^{(29\text{Si})}$ (mT)	54.007(7)	0.572(5)	0.778(5)	1	60.472(5)	147.1(1)	254.3(1)
			55.596(7)	2.935(5)	2	53.906(4)	68.2(8)	202(1)
				58.508(4)	3	53.733(7)	66.7(7)	302(1)
E'_2	\mathbf{g}	2.00035(2)	-0.00005(1)	0.00002(2)	1	2.00158(2)	56.5(6)	91.8(9)
			2.00121(2)	0.00055(2)	2	2.00041(2)	45(6)	320(9)
				2.00075(2)	3	2.00032(2)	64(7)	200(7)
	$\mathbf{A}^{(29\text{Si})}$ (mT)	40.545(7)	0.214(5)	0.113(5)	1	46.841(6)	58.59(4)	87.42(5)
			45.111(7)	2.815(5)	2	40.543(7)	69(5)	191(4)
				42.228(4)	3	40.500(6)	39(4)	309(8)
$\mathbf{A}^{(1\text{H})}$ (mT)	-0.068(9)	0.0028(27)	0.0016(17)	1	0.153(2)	56.1(5)	89(4)	
		0.096(2)	0.084(3)	2	-0.029(4)	33.9(6)	269(60)	
			0.028(3)	3	-0.06(1)	90(30)	359(26)	

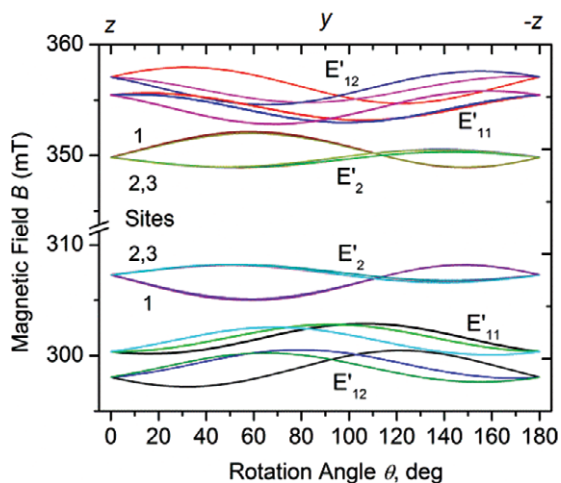


Fig. 5: (Colour online) Angular variation of the $^{29\text{Si}}$ HF line positions for centers E_2 and $E'_{1,1,2}$ as $f(B)$ at the microwave frequency of ~ 9.3 GHz for the rotation of the magnetic field \mathbf{B} in the crystal plane yz . The estimated error in the angle measurement is 0.1° and that in the magnetic field is less than 0.01 mT.

coupling matrix and the nuclear Zeeman splitting, respectively. The best-fit spin Hamiltonian parameters are summarized in table 1.

Our observation of an enhanced E'_1 center at the neutron fluence of 10^{17} n/cm $^{-2}$ is in accordance with previous results on the intensity of paramagnetic defects as a function of the neutron dose [17] where only the E'_1 centers were observed up to 7.5×10^{17} n/cm $^{-2}$. To the best of our knowledge E' -type centers with large HF splitting in $\mathbf{B}||c$ EPR spectra measured along the c -axis were observed only in the work in [16]. Along with $E'_{11,12}$ centers we optimized the EPR parameters for the E'_2 center (note that we use an old designation although in [8] E'_2 was renamed as $E'_2(\text{I})$). In our neutron-irradiated samples the linewidth of E'_2 is broad ($\Delta B_{\text{pp}} \sim 0.07$ mT) in comparison to other E' -type centers. As a consequence, HFS from the weakly interacting proton was poorly resolved even along the c -axis. Also, the weak HF splitting from a proton is not resolved for almost all directions for sites 2 and 3 (fig. 5). However, the proton HF splitting for site 1 reaches a maximum of ~ 0.15 mT near $\theta = 60^\circ$ when the crystal is rotated around the a -axis in the applied magnetic field. Therefore, for the $\mathbf{A}^{(1\text{H})}$ optimization (table 1) we used

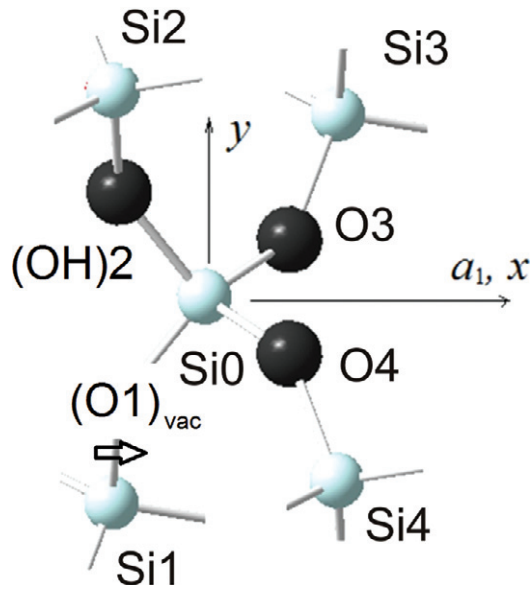


Fig. 6: (Colour online) Fragment of the right-handed α -quartz structure showing a possible model for the E'_2 center with an oxygen vacancy at O1 and an OH group at O2.

mainly data from site 1 and only a few data for the two other sites where the SHFS is clearly resolved. We anticipate that the principal values and directions are correct for A_1 but large uncertainties may exist for A_2 and A_3 principal values and directions.

It is interesting to note that both the principal values and principal directions for E'_2 deviate significantly from those listed in table 3 of ref. [8]. We emphasize that the EPR spectra for E'_2 in ref. [8] were measured about 30 years ago. Also the matrices \mathbf{g} and $\mathbf{A}({}^1\text{H})$ were modified by Persson and Weil [8] in order to be consistent with data from Weeks [7]. This modification might have resulted in the unusual g_1 and $A_1({}^1\text{H})$ principal directions which can be compared with our $A_1({}^{29}\text{Si})$ by a rotation $\varphi + 60^\circ$. Our results show approximately coaxial g_1 , $A_1({}^{29}\text{Si})$, and $A_1({}^1\text{H})$ principal directions (table 1). Furthermore, these directions are approximately along the Si1-O2 (54.3° , 88.8°) structural direction (fig. 6), providing compelling evidence for trapping of the unpaired spin on the Si1 atom. From proton HF coupling in the E'_2 center the silicon-hydrogen internuclear distance was calculated to be ~ 0.5 nm [8]. If hydrogen is bonded to the O2 atom then the distance between Si1 and H would be somewhat larger than $r(\text{Si1-O2})=0.42$ nm, in agreement with the calculated value. Therefore, our new data corroborate the earlier suggestion [7] on the E'_2 model with an unpaired electron trapped on the “long” Si1 dangling bond. Furthermore, we suggest that an OH group located at the O2 position is responsible for the proton SHFS.

However, the structural model for the E'_2 center depicted in fig. 6, without new proton SHFI data, must be considered as tentative.

Recent DFT calculations [1,2,12] showed that the tri-vacancy model with an Al impurity well explains the experimental EPR parameters of the E'_1 and Ge E'_1 centers. But the predicted SHFI with ${}^{27}\text{Al}$ in this model is too small to be resolved in conventional EPR spectroscopy. Our experimental observation of the ${}^{27}\text{Al}$ SHFS (see fig. 4(b)) for the E'_{11} center support the assumption that an Al impurity should be included in the model of some E' -type centers. Unfortunately, we are unable to optimize the ${}^{27}\text{Al}$ SHFI because of its spectral complexity and very low signal-to-noise ratios (*i.e.*, it is difficult to resolve the nuclear transitions). Attempts of EPR measurements for the E'_{11} center at Q -band frequencies (~ 36 GHz) confirmed the ${}^{27}\text{Al}$ SHFS but again did not yield sufficient data points for a quantitative optimization.

The common feature of the $E'_{11,12}$ centers is the orthorhombic \mathbf{g} matrix and the unusually large HFI with ${}^{29}\text{Si}$ ($A_{\text{iso}} = 51.7$ and 56.0 mT for E'_{11} and E'_{12} , respectively). For the E'_{12} center the unique principal directions g_1 , and A_1 are approximately along the Si0-Si1 structural direction (126.1° , 246°). However, the unique principal directions g_1 and A_1 of the E'_{11} center do not match any structural direction. This result may be explained by strong structural distortions because of an Al impurity involved in the defect. It is interesting to note that the observed magnitude of the ${}^{27}\text{Al}$ HFI of the E'_{11} center (fig. 4(b)) is comparable to those of the centers D/E, which are superoxide radicals with the Al impurity located at the next-nearest-neighboring Si site [23].

The new $E'_{11,12}$ centers with large ${}^{29}\text{Si}$ HFI are clearly distinct from all known E' centers in quartz. On the other hand, the orthorhombic \mathbf{g} matrices and the unusually large ${}^{29}\text{Si}$ HFI of the $E'_{11,12}$ centers are similar to those of the E'_α center in amorphous silica [2,14]. Several models have been proposed for the E'_α center [2]. For example, the back-projected configuration interacting with an extra oxygen atom of the α - SiO_2 matrix [14] was supported by embedded cluster calculations [24] which predicted an $A_{\text{iso}}({}^{29}\text{Si}) = 48.9$ mT. However, in [24] g principal values were not calculated permitting the possibility of other configurations for the explanation of E'_α EPR data. Recently [25] the Fermi contact $A_{\text{iso}}({}^{29}\text{Si}) \sim 48$ mT and orthorhombic principal g values calculated for forward-oriented configuration support an assignment of the E'_α as originating from this configuration. The predicted principal g values of 2.0019, 2.0010 and 1.9994 and large A_{iso} for the forward-oriented configuration [25] are closely compatible with our experimental results for the $E'_{11,12}$ centers (table 1). Therefore, the new $E'_{11,12}$ defects observed in neutron-irradiated quartz might be similar to the E'_α center in amorphous silica.

Conclusions. – Single-crystal EPR spectra of natural and synthetic quartz samples after neutron irradiation at two fluences of 5×10^{16} and 5×10^{17} n/cm $^{-2}$ have been investigated. Two new E' -type paramagnetic defects were revealed, including the first-ever observation of the ${}^{27}\text{Al}$

super-hyperfine structure for the E'_{11} center. Hence the Al impurity may be involved in the structural model of some E' -type centers. The two new $E'_{11,12}$ centers are both characterized by orthorhombic \mathbf{g} matrices and large $A_{\text{iso}}(^{29}\text{Si})$ representing analogous defects to the E'_α center in amorphous silica [14,24,25]. For the E'_2 center the primary spin Hamiltonian parameter matrices \mathbf{g} and $\mathbf{A}(^{29}\text{Si})$ have been refined.

REFERENCES

- [1] MASHKOVITSEV R. I. and PAN Y., in *New Developments in Quartz: Varieties, Crystal Chemistry and Uses in Technology*, edited by NOVACK B. and MAREK P. (Nova Science Publishers, New York) 2013, Chapt. 2, pp. 65–104.
- [2] ALESSI A. *et al.*, in *Applications of EPR in Radiation Research*, edited by LUND A. and SHIOTANI M. (Springer International Publishing, Cham) 2014, Chapt. 7, pp. 255–295.
- [3] MASHKOVITSEV R. I. and PAN Y., *Phys. Chem. Miner.*, **38** (2011) 647.
- [4] MASHKOVITSEV R. I. and PAN Y., *EPL*, **98** (2012) 56005.
- [5] MASHKOVITSEV R. I. and PAN Y., *EPL*, **107** (2014) 36005.
- [6] SILSBEE R. H., *J. Appl. Phys.*, **32** (1961) 1459.
- [7] WEEKS R. A., *Phys. Rev.*, **130** (1960) 570.
- [8] PERLSON B. D. and WEIL J. A., *Can. J. Phys.*, **86** (2008) 871.
- [9] ISOYA J., WEIL J. A. and HALLIBURTON L. E., *J. Chem. Phys.*, **74** (1981) 5436.
- [10] MASHKOVITSEV R. I. and PAN Y., *Phys. Chem. Miner.*, **39** (2012) 79.
- [11] FEIGL F. J. and ANDERSON J. H., *J. Phys. Chem. Solids*, **31** (1970) 575.
- [12] MASHKOVITSEV R. I. *et al.*, *J. Magn. Reson.*, **233** (2013) 7.
- [13] WEEKS R. A., MAGRUDER R. H. and STESMANS A., *J. Non-Cryst. Solids*, **354** (2008) 208.
- [14] BUSCARINO G., AGNELLO S. and GELARDI F. M., *Phys. Rev. Lett.*, **97** (2006) 135502.
- [15] WEEKS R. A. and NELSON C. M., *J. Am. Ceram. Soc.*, **43** (1960) 399.
- [16] SOLNTSEV V. P., MASHKOVITSEV R. I. and SHCHERBAKOVA M. YA., *J. Struct. Chem.*, **18** (1977) 578.
- [17] JANI M. G. and HALLIBURTON L. E., *J. Appl. Phys.*, **56** (1984) 942.
- [18] TOYODA S. and SCHWARCZ H. P., *Radiat. Meas.*, **27** (1997) 59.
- [19] BARTOLL J., SCHWARCZ H. P. and RINK W. J., *Radiat. Meas.*, **33** (2001) 893.
- [20] FENG P. B. *et al.*, *Phys. Lett. A*, **376** (2012) 2195.
- [21] NILGES M. J., PAN Y. and MASHKOVITSEV R. I., *Phys. Chem. Miner.*, **35** (2008) 221.
- [22] PAN Y., NILGES M. J. and MASHKOVITSEV R. I., *Phys. Chem. Miner.*, **35** (2008) 387.
- [23] PAN Y., NILGES M. J. and MASHKOVITSEV R. I., *Mineral. Mag.*, **73** (2009) 519.
- [24] MUKHODPADHYAY S. *et al.*, *Phys. Rev. B*, **70** (2004) 195203.
- [25] GIACOMAZZI L. *et al.*, *Phys. Rev. B*, **90** (2014) 014108.